RCSLenS galaxy cross-correlations with WiggleZ and BOSS

Chris Blake, 24 June 2013

1 Scope

The scope of this investigation is to measure the cross-correlation between RCSLenS shapes (two-thirds of which have photometric redshifts) and WiggleZ and BOSS DR9 lenses (with spectroscopic redshifts) at intermediate scales ($> 1\,h^{-1}$ Mpc) across redshift range $z < 1$ *[Note: the BOSS sample will soon be updated to DR10]*. Galaxy bias and σ_8 will be fit to the angular shape-density cross-correlation $\gamma_t(\theta)$ and the projected shape-density cross-correlation $\Delta\Sigma(R)$, in combination with the projected lens auto-correlation $w_p(r_p)$. The E_G parameter (Zhang et al. 2007, Reyes et al. 2010) will be calculated taking WiggleZ and BOSS measurements of the redshift-space distortion parameter β as an external input. Covariance matrices obtained from jack-knife re-sampling and from scaling the existing CFHTLenS CLONE simulations will be compared. A more complete analysis, self-consistently including the redshift-space distortion information, computing a more rigorous covariance using new mock catalogues, and performing full cosmological parameter fits, will be left to future work.

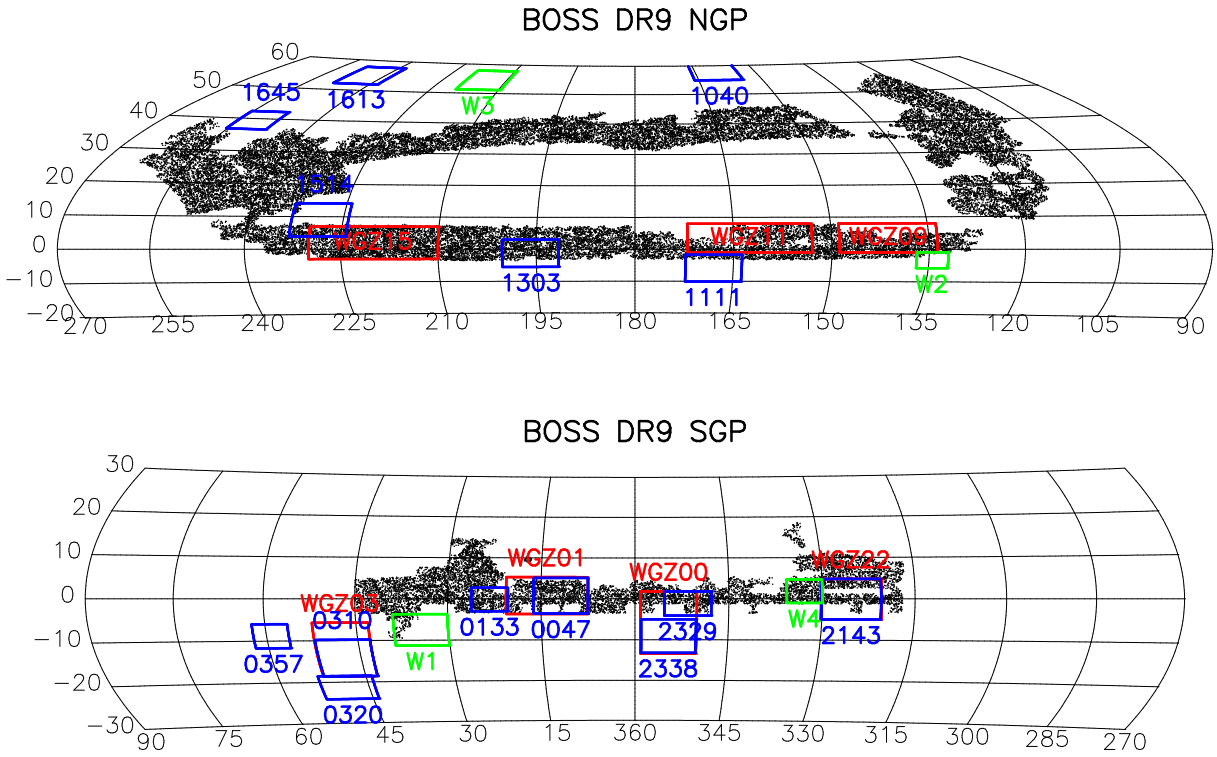

Figure 1: (R.A., Dec.) distribution in the NGP and SGP of the SDSS DR9 (BOSS) galaxy sample (black dots), the WiggleZ survey regions (red rectangles), the RCSLenS fields (blue rectangles) and the CFHTLenS fields (green rectangles).

2 Data

2.1 Sky coverage and lens redshift distribution

Figure 1 displays the sky distribution of the RCSLenS, WiggleZ and BOSS (DR9) datasets used in this analysis *[Note: the BOSS sample will soon be updated to DR10]*. Figure 2 plots the number density distribution with redshift of the lenses. Table 1 lists the statistics of each RCSLenS region analyzed including the total effective (unmasked) area, the areas passing the cosmology-independent systematics cull of pointings, the areas containing photo-z information, the source density and the number of lenses *[Note: the cosmology-independent systematics tests for RCSLenS still need to be finalized?]*. The RCSLenS regions used for cross-correlation with (WiggleZ, BOSS) contain an effective area of (244, 217) deg^2, of which (160, 149) deg^2, i.e. around two-thirds, contains 4-band photometric redshifts.

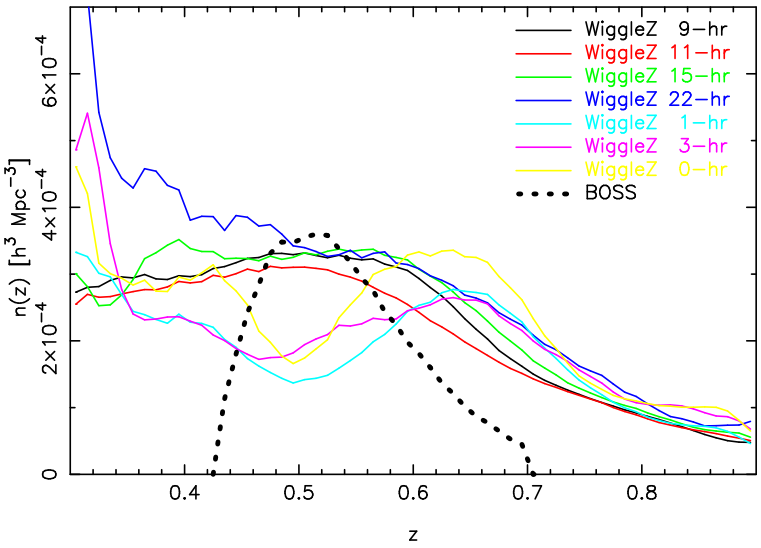

Figure 2: Number density distribution with redshift of lenses in each WiggleZ survey region and in BOSS. The redshift distribution differs between WiggleZ regions because of varying colour/magnitude selection and completeness of spectroscopic follow-up.

2.2 Source selection

The following cuts are applied to the RCSLenS source catalogues for inclusion in the cross-correlation analysis:

- Within good area of data: $CANDIDATEMASK = 0$
- Magnitude threshold: $MAG\_AUTO - EXTINCTION\_r < 24$
- Star-galaxy cut: $SG\_FLAG = 1$
- Lensfit weight: $WEIGHT > 0$
- For $\Delta\Sigma(R)$ analysis, good photometric redshift: $(0.2 < Z_B < 0.45$ AND $ODDS > 0.8)$ OR $(Z_B > 0.45)$. Photo-z's with $Z_B < 0.2$ are not considered reliable.

Table 1: Statistics for RCSLenS regions cross-correlated with WiggleZ and BOSS data; the source density is evaluated for $MAG\_AUTO < 24$ *[Note: there is a mistake here, I didn't do an extinction correction when compiling this table].* Effective (unmasked) areas are shown for the full region, the set of pointings passing the cosmology-independent systematics cull, and the pointings which contain 4 filters such that photometric redshifts are available. We note that the source densities are lower for the photo-z sample because of the cuts applied in the $ODDS$ parameter. We only cross-correlate the four RCSLenS regions for each spec-z sample with significant overlap.

WiggleZ field	$A_{\rm eff}$[all] [deg^2]	$A_{\rm eff}$[no-sys] [deg^2]	$A_{\rm eff}$[photo-z] [deg^2]	$\sigma_{\rm source}$ [arcmin^{-2}]	$N_{\rm lens}$	Use?
0047	54.5	49.0	37.7	3.93	17,111	Yes
0310	63.5	46.8	54.6	3.70	19,076	Yes
1514	61.3	56.1	31.9	4.22	3,712	No
2143	65.5	51.9	47.0	4.27	30,892	Yes
2329	35.4	31.8	32.6	4.61	2,274	No
2338	60.7	53.5	20.7	3.86	17,136	Yes
BOSS field	$A_{\rm eff}$[all] [deg^2]	$A_{\rm eff}$[no-sys] [deg^2]	$A_{\rm eff}$[photo-z] [deg^2]	$\sigma_{\rm source}$ [arcmin^{-2}]	$N_{\rm lens}$	Use?
0047	54.5	49.0	37.7	3.93	4,525	Yes
0133	27.1	21.6	14.0	3.47	2,273	No
1303	13.2	10.1	8.4	4.25	4,087	No
1514	61.3	56.1	31.9	4.23	2,739	Yes
2143	65.5	51.9	47.0	4.27	3,890	Yes
2329	35.4	31.8	32.6	4.62	2,544	Yes

BPZ photometric redshifts are used in the analysis, for which full probability distributions PZ_full are available for each source. We note that the value of e_2 listed in the source catalogues must be reversed in our cross-correlation pipeline, because the positive x-direction of pixel co-ordinates lies in the negative R.A. direction.

2.3 Determination of source spectroscopic redshift distribution $P(z_s)$

The spec-z distribution of all RCSLenS sources is calculated by scaling the well-determined distributions from CFHTLenS as a function of magnitude, weighting by RCSLenS lensfit weights *[Note: need to check this].* Figure 3 shows the redshift distributions for magnitude thresholds $m < 24$ (representative of the data) and $m < 23$ (currently used to sub-sample the CLONE source distribution). A separate spec-z distribution is determined for the photo-z sample by summing the BPZ probability distributions of the sources included in the sample, weighting by the lensfit weights. This is also shown in Figure 3.

2.4 Determination of source photometric redshift model $P(z_p|z_s)$

The function $P(z_p|z_s)$ is required in order to introduce photo-z errors to the mock catalogues for testing the pipeline. This function was determined by a Monte Carlo method as follows: for each source passing the photo-z cuts, a spectroscopic redshift z_s was drawn at random from the distribution PZ_full. The values (z_p, z_s) were then binned, weighting each galaxy by the lensfit

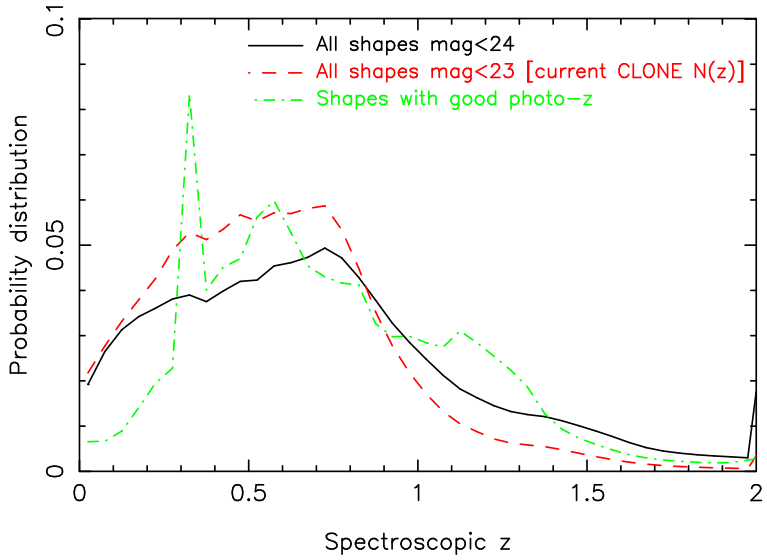

Figure 3: Spec-z probability distribution models used for the whole RCSLenS data shape sample (solid black line), the current CLONE shape $N(z)$ (dashed red line), and the sample of good photo-z's (dot-dashed green line).

weight, and the distribution over z_p was determined for each z_s bin. A greyscale representation of $P(z_p|z_s)$ is shown in Figure 4.

2.5 CLONE simulations

For testing our methods and estimating the covariance matrix of measurements, we use the CLONE simulations generated for the CFHTLenS project, which provide density fields and ray-traced shape distributions for 184 lines-of-sight, each covering 12.85 deg^2. A large number of sources have been randomly positioned across each field with a redshift distribution matched to CFHTLenS $m = 23$ as shown in Figure 3 *[Note: this needs updating for RCSLenS]*.

We sample the CLONE density fields with $b = 1$ and $b = 2$ tracers to approximate the linear bias properties of the WiggleZ and BOSS lenses, with redshift distributions matching those surveys as shown in Figure 2. We note that a bias model with $b > 1$ cannot be applied self-consistently on all scales because then the galaxy density field ρ_g contains negative regions; once a condition is imposed that $\rho_g = max(\rho_g, 0)$ then the effective value of the large-scale bias is reduced. We experimented with alternative approaches including smoothing the density field before applying the $b = 2$ sub-sampling. We sub-sample the simulations to match the average source density and number of lenses in each RCSLenS region.

Shape noise with $\sigma_e = 0.29$ is applied to the CLONE source catalogues using the following method:

- A complex noise $n = n_1 + n_2\, i$ is formed for each source, where n_1 and n_2 are drawn from Gaussian distributions with standard deviation σ_e.
- A complex shear $\gamma = \gamma_1 + \gamma_2\, i$ is formed from the shear components (γ_1, γ_2) obtained from the ray-tracing.
- A complex noisy ellipticity is determined as $e = (\gamma + n)/(1 + n\,\gamma^*)$. The components of the observed ellipticity (e_1, e_2) are then found as $e = e_1 + e_2\, i$.

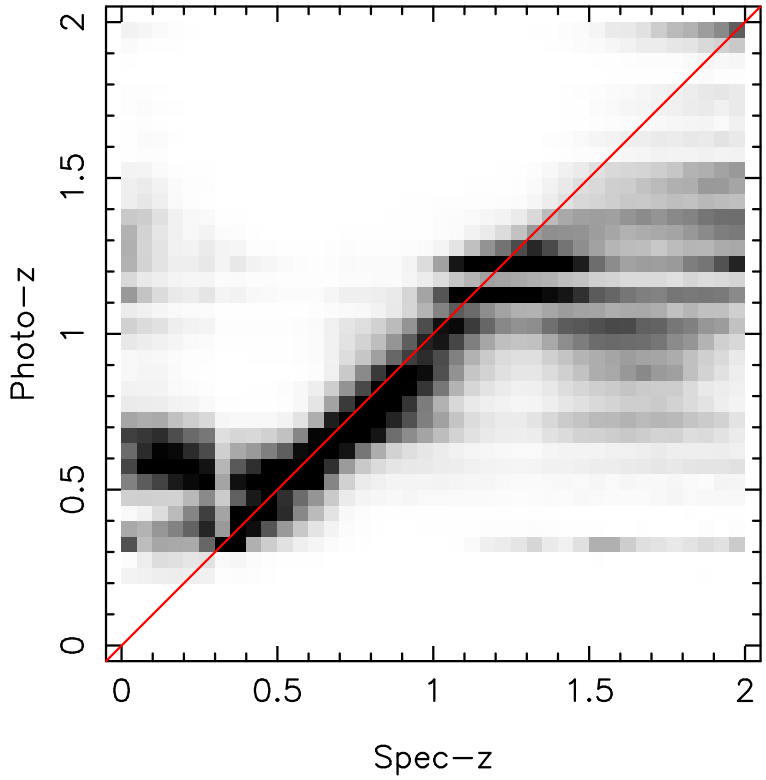

Figure 4: A greyscale representation of the function $P(z_p|z_s)$ which describes the photo-z probability distribution as a function of spec-z, determined by a Monte Carlo sampling of the photo-z probability distributions of each source appearing in the catalogue.

We note a couple of properties of the CLONE simulations: the box-size for $z < 1 (z > 1)$ is $L = 147(231)\,h^{-1}$ Mpc hence the matter power spectrum $P(k)$ of the simulations is zero for $k < 2\pi/L = (0.043, 0.027)\,h$ Mpc^{-1}. Hence the simulations will under-estimate the clustering strength of a real data sample on large scales ($\theta > 40$ arcmin). Also, the density fields along each line-of-sight are constructed from a series of 26 redshift snapshots such that $P(k, z)$ is a stepwise function of z. These properties are included when generating model cross-correlation functions for testing the self-consistency of the methodology.

We also constructed mock catalogues for each RCSLenS region including the full survey mask of sources and lenses, implemented by stitching together multiple lines-of-sight for the CLONE simulations and sub-sampling the result to match the survey selection functions. 20 realizations of each survey region can be generated from the 184 CLONE simulations. This masked simulation set allows a comparison of diagonal measurement errors to be performed, to understand the importance of the survey selection function in the measurement error. The sky distributions of the sources and lenses for the data and simulation for the WiggleZ-RCSLenS 2143 region are compared in Figure 5.

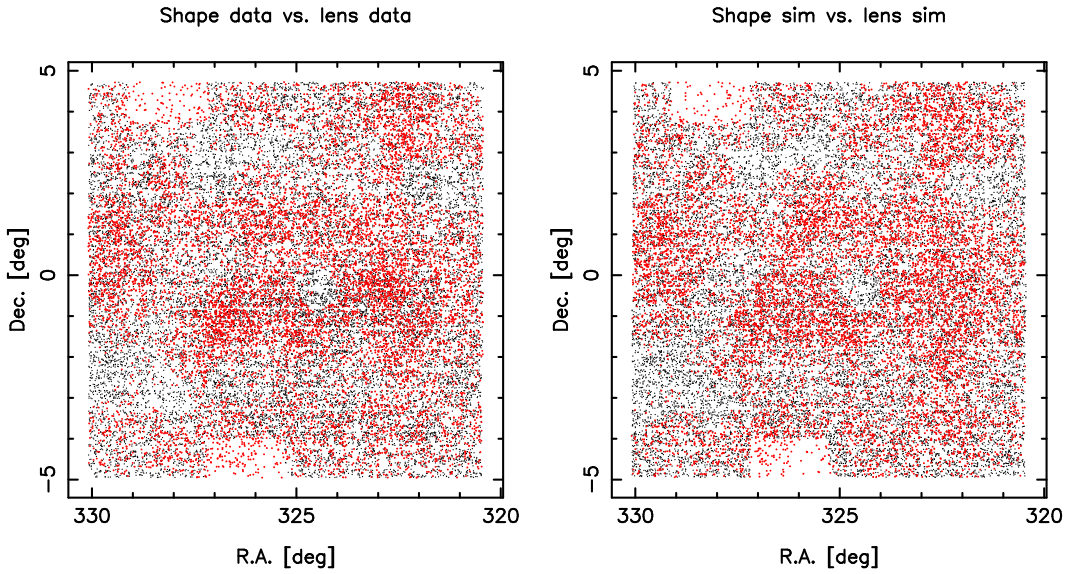

Figure 5: Comparison of the distributions of the source and lens data and corresponding masked simulation in the WiggleZ-RCSLenS 2143 region. The galaxies have been sub-sampled for ease of plotting.

3 Cross-correlation measurements

3.1 Measurement of $\gamma_t(\theta)$

We first measured the angular cross-correlation $\gamma_t(\theta)$ of the galaxy-galaxy lensing signal. The components of ellipticity $(e_{1,i}, e_{2,i})$ of source i relative to the positive x-axis are defined by

$$(e_1, e_2) = \left(\frac{\beta - 1}{\beta + 1}\right)(\cos 2\psi, \sin 2\psi) \tag{1}$$

where ψ is the position angle of a galaxy with axial ratio β measured anti-clockwise from the positive x-axis. These ellipticity components can be rotated to new values $[e_t(i,j), e_\times(i,j)]$ relative to a line connecting sources i and j by

$$e_t(i,j) = -e_{1,i}\cos 2\phi(i,j) - e_{2,i}\sin 2\phi(i,j) \tag{2}$$

$$e_\times(i,j) = e_{1,i}\sin 2\phi(i,j) - e_{2,i}\cos 2\phi(i,j) \tag{3}$$

where $\phi(i,j)$ is the angle of the line connecting sources i and j to the positive x-axis (e.g., in the range $-90° < \phi < 90°$). Our galaxy-galaxy lensing estimators are then:

$$\gamma_t(\theta) = \frac{\sum_{\text{sources}\,i}\sum_{\text{lenses}\,j} w_i^s\, w_j^l\, e_t(i,j)\,\Theta(i,j)}{\sum_{\text{sources}\,i}\sum_{\text{lenses}\,j} w_i^s\, w_j^l\,\Theta(i,j)} \tag{4}$$

$$\gamma_\times(\theta) = \frac{\sum_{\text{sources}\,i}\sum_{\text{lenses}\,j} w_i^s\, w_j^l\, e_\times(i,j)\,\Theta(i,j)}{\sum_{\text{sources}\,i}\sum_{\text{lenses}\,j} w_i^s\, w_j^l\,\Theta(i,j)} \tag{5}$$

where w_i^s is the lensfit weight of shape i, $\Theta(i,j)$ is equal to 1 if the angular separation between sources i and j lies in bin θ, and equal to 0 otherwise, w_i^l is the weight of lens galaxy i (currently set to $w^l = 1$ for WiggleZ and the catalogued values for BOSS), and the sums are taken over unique pairs.

Figure 6 shows the measurements of tangential shear $\gamma_t(\theta)$ and cross shear $\gamma_\times(\theta)$ obtained by combining the separate WiggleZ and BOSS fields listed in Table 1, for the data and the mock mean of the CLONE catalogues. The solid line is the model prediction for the CLONE simulation, which is included only for comparison with the mock mean. The BOSS mock mean falls systematically below the model, owing to the issue with generating $b = 2$ mocks mentioned above. We performed measurements in 20 logarithmically-spaced angular bins from $\theta = 0.01°$ to $1°$. The cross shear measurement is consistent with the expectation of zero for both the data and mocks, with χ^2 values of $(20.3, 11.8)$ for the (WiggleZ, BOSS) data for 20 degrees of freedom. The covariance matrices for these calculations are determined using the 184 CLONE lines-of-sight and scaling by effective area, as described below.

Figure 7 shows measurements of $\gamma_t(\theta)$ from the data and CLONE mocks split into four redshift slices of WiggleZ lenses, $(0.1 < z < 0.3, 0.3 < z < 0.5, 0.5 < z < 0.7, 0.7 < z < 0.9)$.

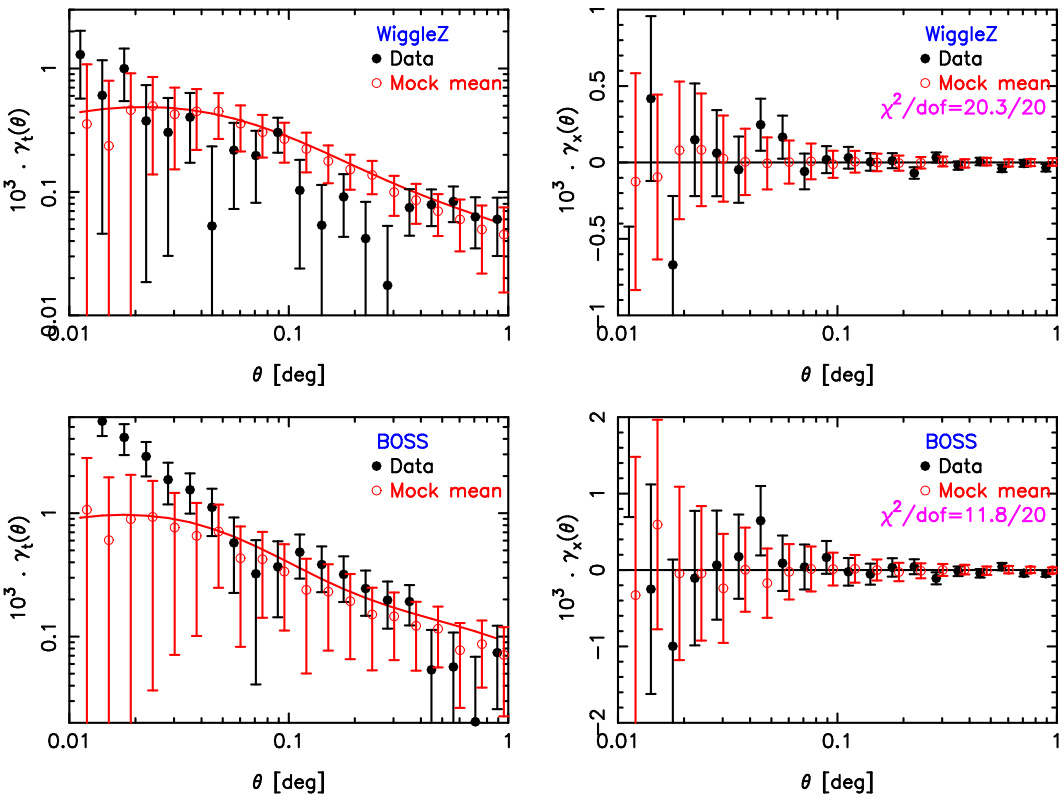

Figure 6: Measurements of $\gamma_t(\theta)$ (left column) and $\gamma_\times(\theta)$ (right column) for the cross-correlation of RCSLenS sources with WiggleZ lenses (top row) and BOSS lenses (bottom row). We show results for the data and the mock mean. The overplotted model is included only for comparison with the mock mean. χ^2 statistics are quoted for the WiggleZ and BOSS $\gamma_\times$ measurements with respect to a model of zero.

3.2 Error estimation for $\gamma_t(\theta)$

We compare three techniques for obtaining errors in the measurement of $\gamma_t(\theta)$:

- Jack-knife errors, where 16 (4×4) jack-knife regions of typical dimension ~ 2 deg are used per RCSLenS region, obtained by dividing the source distribution into sub-samples containing equal number of galaxies using constant R.A. and Dec. boundaries.

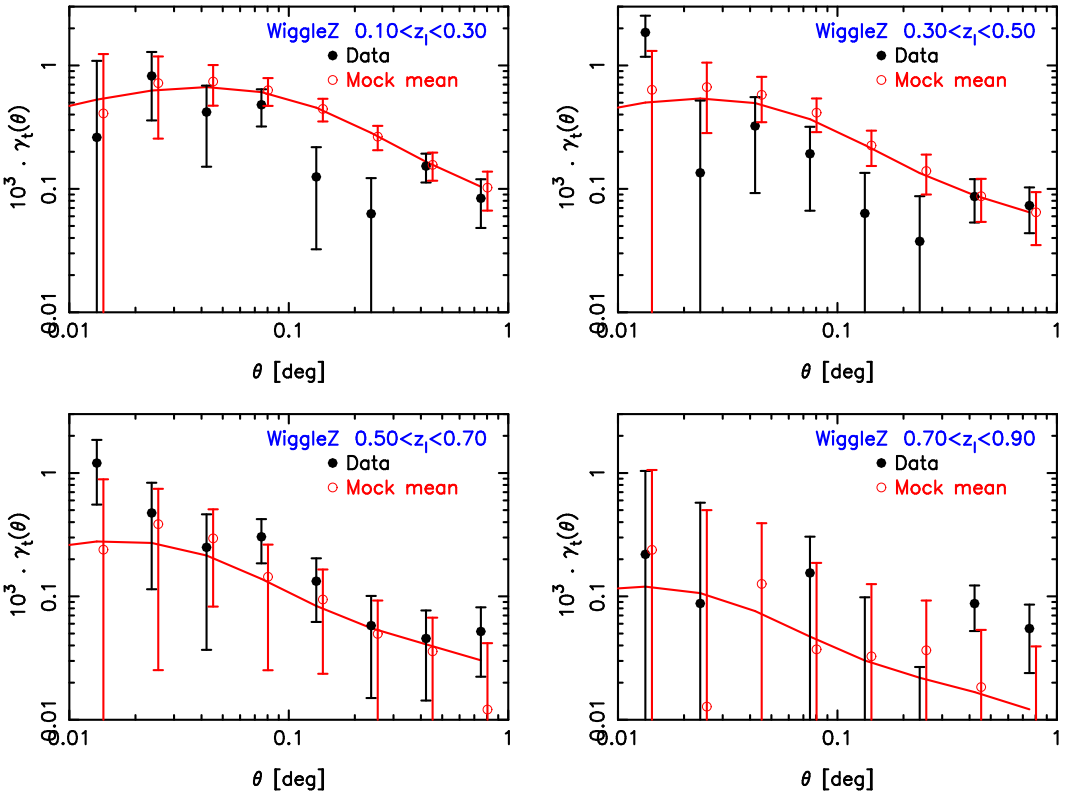

Figure 7: Measurements of $\gamma_t(\theta)$ for the cross-correlation of RCSLenS sources with WiggleZ lenses in four redshift slices. We show results for the data and the mock mean. The overplotted model is included only for comparison with the mock mean.

- Simulated errors not including the survey mask. We used the CLONE simulations discussed above, which comprise 184 lines-of-sight each covering 12.85 deg^2. We measure cross-correlations for each line-of-sight, and scale the resulting scatter by $\sqrt{12.85/A_{\rm eff}}$ where $A_{\rm eff}$ is the effective (unmasked) area of each RCSLenS region listed in Table 1.
- Simulated errors including the survey mask, implemented by stitching together multiple lines-of-sight for the CLONE simulations and sub-sampling the result to match the selection functions of the sources and the lenses. 20 realizations of each survey region were generated from the 184 CLONE simulations.

Figure 8 compares these error determinations, combining results in the different WiggleZ and BOSS regions. Agreement between the data jack-knife errors and both types of simulation is good at $\theta < 0.4$ deg. The error determined from the area-scaled unmasked simulations and fully-masked simulations matches for all angles, and is lower than the data jack-knife errors. We note that the simulations may under-estimate the true clustering at $\theta > 0.7$ deg because of the limited box size. The jack-knife method applied to the simulations including the full selection functions matches that obtained from the data itself. Figure 9 displays the covariance matrix in different θ bins determined from the area-scaled 184 CLONE WiggleZ simulations. The covariance between different angular bins is low, apart from scales $\theta > 0.5$ deg.

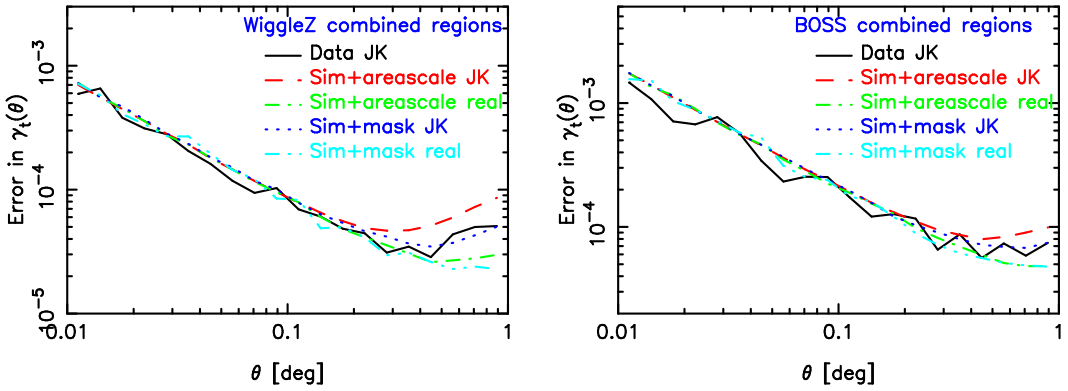

Figure 8: Comparison of the errors in $\gamma_t(\theta)$ determined by jack-knife re-sampling of the data, by using the 184 CLONE lines-of-sight and scaling by an effective area factor (comparing jack-knife re-sampling of the simulations and the scatter between the realizations), and by generating 20 simulations of each region including the full selection functions (comparing jack-knife re-sampling and the realization scatter).

3.3 Measurement of $\Delta\Sigma(R)$

We also measured the differential projected surface density $\Delta\Sigma(R)$ around the lenses as a function of transverse co-moving separation R. This quantity is harder to interpret from a theoretical perspective than $\gamma_t(\theta)$, but permits a constant projected co-moving scale to be matched across different redshifts, and allows for comparison with other investigations such as Reyes et al. (2010) and Mandelbaum et al. (2012).

$\Delta\Sigma(R)$ is defined in terms of the projected surface density $\Sigma(R)$ by $\Delta\Sigma(R) = \overline{\Sigma}(< R) - \Sigma(R)$ where $\overline{\Sigma}(< R) = \frac{2}{R^2}\int_0^R R'\,\Sigma(R')\,dR'$. It is related to the lens galaxy-matter cross-correlation function $\xi_{gm}(r)$ by

$$\Delta\Sigma(R) = \overline{\rho}_m \int \xi_{gm}(\sqrt{R^2+\pi^2})\,d\pi \tag{6}$$

where $\overline{\rho}_m$ is the mean matter density, and to the observable tangential shear distortion $\gamma_t(\theta)$ of a single source-lens pair with redshifts (z_s, z_l) by

$$\Delta\Sigma(R, z_l) = \gamma_t(\theta)\,\Sigma_c(z_s, z_l) \tag{7}$$

where the geometric "lensing efficiency" Σ_c is given by

$$\Sigma_c(z_s, z_l) = \frac{c^2}{4\pi G}\left[\frac{x_s}{(x_s - x_l)\,x_l\,(1+z_l)}\right] \tag{8}$$

$$= \frac{2}{3}\frac{c}{H_0}\frac{3H_0^2}{8\pi G}\left[\frac{x_s\,(c/H_0)}{(x_s - x_l)\,x_l\,(1+z_l)}\right] \tag{9}$$

$$= 554.65\,h\,M_\odot\,\mathrm{pc}^{-2}\left[\frac{x_s\,(c/H_0)}{(x_s - x_l)\,x_l\,(1+z_l)}\right] \tag{10}$$

where x_s and x_l are the co-moving radial co-ordinates (in a flat Universe) of the source and lens. Given that the lens galaxy-matter cross-correlation function ξ_{gm} scales with redshift in proportion to $b(z)\,G(z)^2$, in terms of the linear galaxy bias factor $b(z)$ and linear growth factor $G(z)$, for a broad lens distribution we can write an estimator of $\Delta\Sigma(R)$ for $b = 1$ galaxies at $z = 0$ as

$$\Delta\Sigma(R, 0) = \frac{\gamma_t(\theta)\,\Sigma_c(z_s, z_l)}{b(z_l)\,G(z_l)^2} = K_{ls}\,\gamma_t(\theta) \tag{11}$$

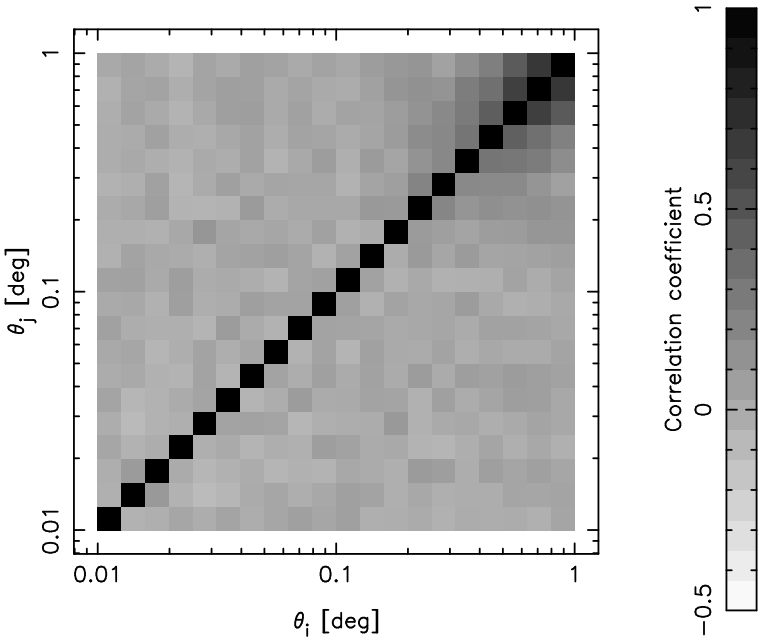

Figure 9: Covariance matrix of the $\gamma_t(\theta)$ measurements determined using the scatter across the 184 CLONE simulation lines-of-sight, displayed as a correlation matrix $C_{ij}/\sqrt{C_{ii}C_{jj}}$.

where the error in the estimate of $\Delta\Sigma(R,0)$ from a single pair is proportional to $K_{ls} = \Sigma_c(z_s,z_l)/[b(z_l)\,G(z_l)^2]$ (this approach is used for convenience to allow the WiggleZ and BOSS cross-correlations, with different lens galaxy bias factors and redshifts, to be easily compared; we assumed $b(z) = 1$ for WiggleZ and $b(z) = 2$ for BOSS). *[Note: will probably change this approach for the final version, it is a bit weird!]* The optimal inverse-variance weight for each lens-source pair is then $w_{ls} = 1/K_{ls}^2$.

Our method for measuring $\Delta\Sigma(R)$ from the samples is:

- Restrict the source sample to those with "good" photometric redshifts as described above.
- Identify pairs of lenses and sources that are physically close on the sky (using the co-moving transverse separation at the lens redshift, $R = x_l\,\theta$) and satisfy $z_s > z_l$ (using the photometric source redshift and spectroscopic lens redshift).
- Give each pair a weight $(w_l\,w_s\,w_{ls})$ where w_l is the weight of the lens galaxy (currently set to $w_l = 1$ for WiggleZ and the catalogue values for BOSS), w_s is the lensfit weight of the source galaxy, and $w_{ls} = K_{ls}^{-2} \propto \Sigma_c^{-2}$, defined above, is the inverse variance of the expected lensing signal-to-noise ratio of this pair.
- Compute the lensing signal in a series of annular bins

$$\Delta\Sigma(R) = \frac{\sum_{ls\,\mathrm{pairs}} w_l\,w_s\,w_{ls}\,\gamma_t\,\Sigma_c(z_s,z_l)/b(z_l)G(z_l)^2}{\sum_{ls\,\mathrm{pairs}} w_l\,w_s\,w_{ls}} \tag{12}$$

Figure 10 shows the measurement of $\Delta\Sigma(R)$ in 12 logarithmically spaced bins in R from 0.1 to $100\,h^{-1}$ Mpc, obtained by combining the separate WiggleZ and BOSS fields listed in Table 1, for the data and the mock mean of the CLONE catalogues. The solid line is the model prediction for the CLONE simulation, which is included only for comparison with the mock mean.

Figure 11 shows measurements of $\Delta\Sigma(R)$ from the data and CLONE mocks split into four redshift slices of WiggleZ lenses, $(0.1 < z < 0.3, 0.3 < z < 0.5, 0.5 < z < 0.7, 0.7 < z < 0.9)$.

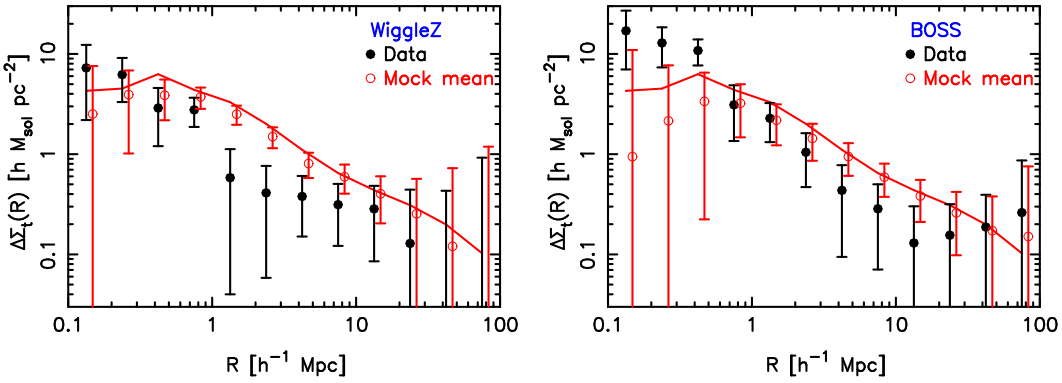

Figure 10: $\Delta\Sigma(R)$ measured for the cross-correlation of WiggleZ and BOSS lenses with RCSLenS sources. We show results for the data and the mock mean. The overplotted model is included only for comparison with the mock mean.

3.4 Error estimation for $\Delta\Sigma(R)$

We compared the errors in $\Delta\Sigma(R)$ determined using the three techniques described above: jack-knife data errors, area-scaled measurements of the 184 lines-of-sight of the CLONE simulations, and measurements from 20 realizations combining together the CLONE simulations including the selection function of the sources and lenses. For the simulated measurements of $\Delta\Sigma(R)$ we sub-sampled the source density in each region to match that of the data with good photometric redshifts. We note that following this cut, the redshift distribution of the simulated sources may not match that of the data *[Note: this needs to be fixed!]*. For the area-scaling we used the area of the good photo-z pointings (listed in Table 1); this may over-estimate the errors because we still included lens-source pairs involving lenses in the pointings without photometric redshifts, such that the true effective area is larger than that assumed here.

Figure 12 compares these error determinations, combining results in the different WiggleZ and BOSS regions. The error from the data jack-knife lies systematically below the simulated errors, possibly for one or more of the reasons described above. Errors obtained from the various simulation approaches agree well for $R < 2\,h^{-1}$ Mpc. For scales $R > 20\,h^{-1}$ Mpc, the predictions of the area-scaled simulations diverge from those of the masked simulations, possibly because the clustering measurement from the masked simulations includes pairs which straddle different CLONE lines-of-sight, for which the intrinsic clustering is under-estimated. Figure 13 displays the covariance matrix in different R bins determined from the area-scaled 184 CLONE WiggleZ simulations. The covariance between different bins is more significant than that measured for the angular cross-correlations plotted in Figure 9, and becomes large for $R > 10\,h^{-1}$ Mpc.

3.5 Measurement of $w_p(R)$

We additionally measured the 2D lens galaxy correlation function $\xi(R, \pi)$, binning galaxy pairs by projected separation R and line-of-sight separation π. We hence determine the projected

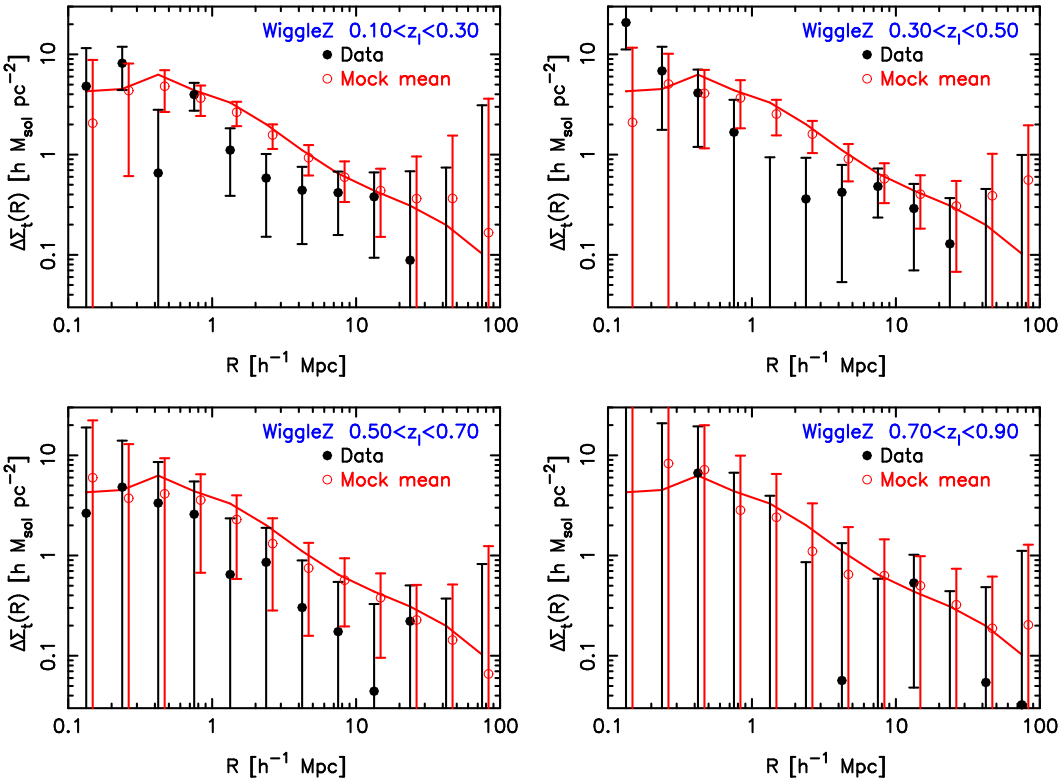

Figure 11: Measurements of $\Delta\Sigma(R)$ for the cross-correlation of RCSLenS sources with WiggleZ lenses in four redshift slices. We show results for the data and the mock mean. The overplotted model is included only for comparison with the mock mean.

correlation function

$$w_p(R) = \sum_{\text{bins}\, i} \xi_{gg}(R, \pi_i)\, \Delta\pi_i \tag{13}$$

where we sum over 10 logarithmically-spaced bins in π from 0.1 to $60\,h^{-1}$ Mpc. The measurements of $w_p(R)$ for the WiggleZ lenses in redshift slices are plotted in Figure 14. No measurements are possible for the CLONE simulations because the lenses are selected from a projected density field and lack spectroscopic redshifts. The errors displayed in Figure 14 are therefore jack-knife errors.

3.6 Measurement of $\Upsilon_{gm}(R)$ and $\Upsilon_{gg}(R)$

[Note: This work is on hold awaiting the data and mocks to be finalized].

Mandelbaum et al. define the annular differential surface density

$$\Upsilon_{gm}(R, R_0) = \Delta\Sigma(R) - \frac{R_0^2}{R^2}\,\Delta\Sigma(R_0) \tag{14}$$

in order to (partially) suppress small-scale contributions to $\Delta\Sigma(R)$, where R_0 is a small-scale cut-off. $\Delta\Sigma(R_0)$ is determined by a power-law fit to $\Delta\Sigma(R)$ over a limited range of scales $R \sim R_0$ (we take the fitting range as $R_0/3 < R < 3R_0$). We assume $R_0 = 1\,h^{-1}$ Mpc for our analysis.

The corresponding quantity for the galaxy auto-correlations is

$$\Upsilon_{gg}(R, R_0) = \rho_c \left[\frac{2}{R^2} \int_{R_0}^{R} R'\, w_p(R')\, dR' - w_p(R) + \frac{R_0^2}{R^2} w_p(R_0) \right] \tag{15}$$

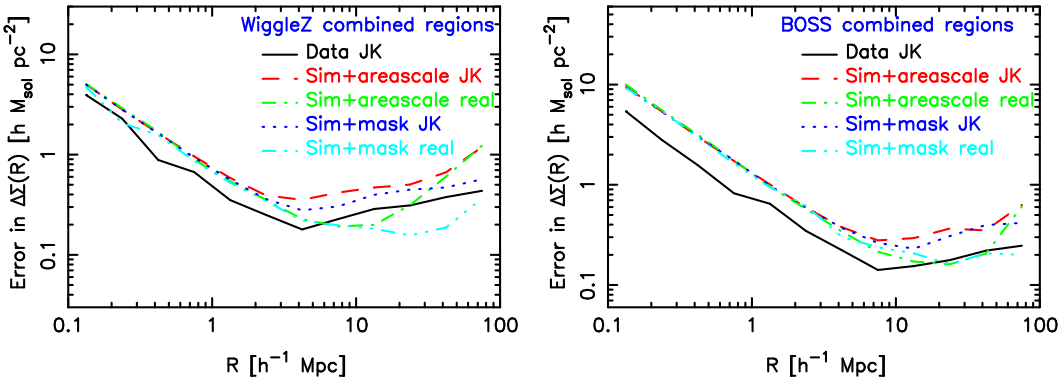

Figure 12: Comparison of the errors in $\Delta\Sigma(R)$ in the same manner as Figure 8.

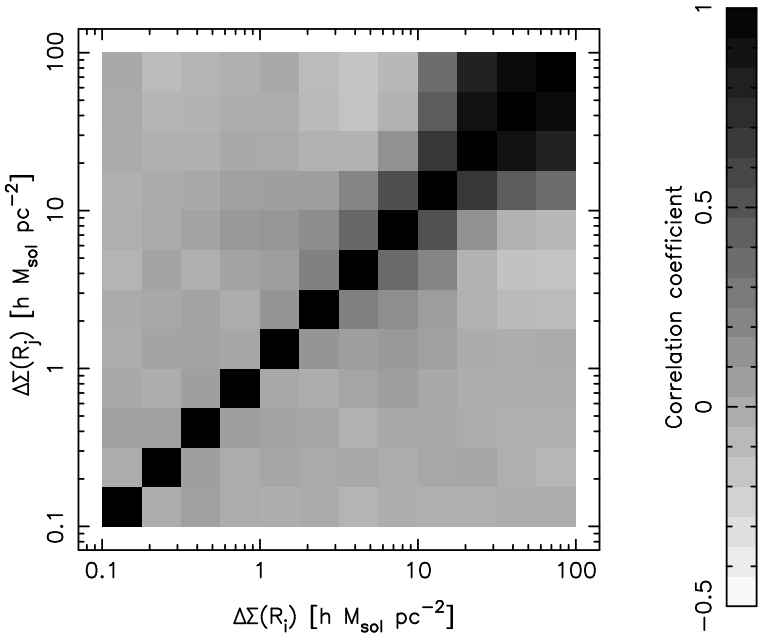

Figure 13: Covariance matrix of the $\Delta\Sigma(R)$ measurements determined using the scatter across the 184 CLONE simulation lines-of-sight, displayed as a correlation matrix $C_{ij}/\sqrt{C_{ii}C_{jj}}$.

where $\rho_c = 2.77518 \times 10^{11}\, h^2 M_\odot$ Mpc^{-3} is the critical density of the Universe. We determine $w_p(R_0)$ using a power-law fit over the same range as above, and evaluate the integral appearing in the first term of the above equation using a spline fit to the measured $w_p(R)$.

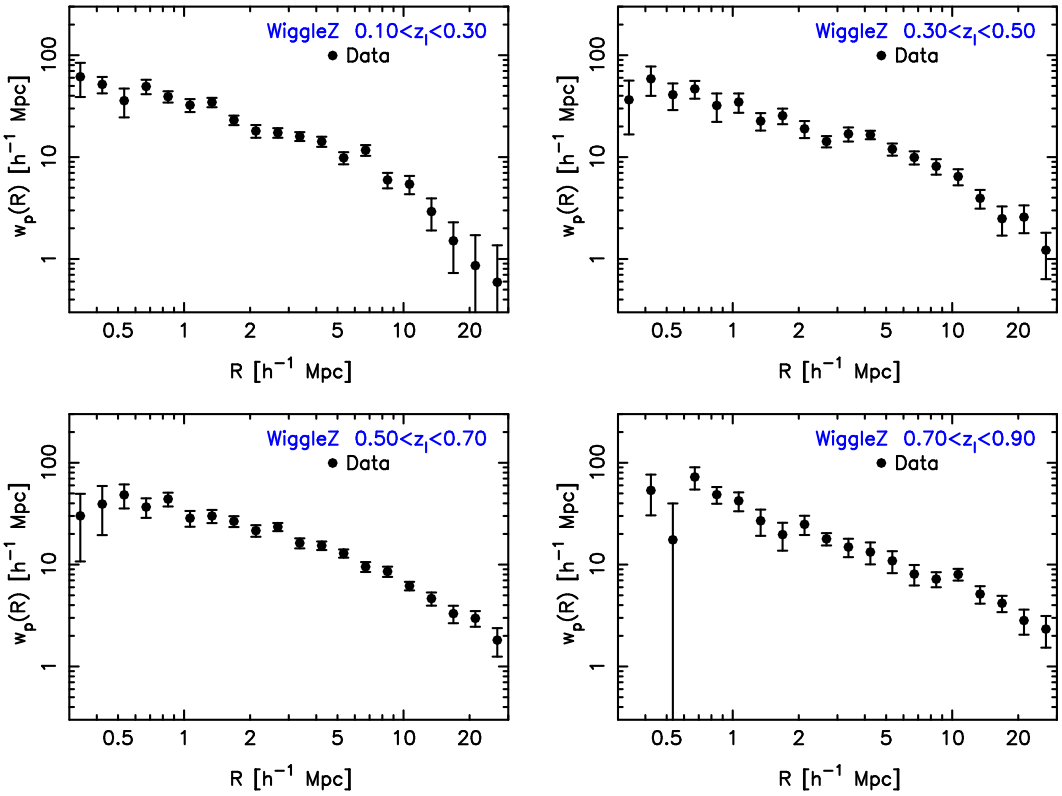

Figure 14: The projected correlation function $w_p(R)$ for the WiggleZ lens catalogues in redshift slices. Jack-knife errors are plotted.

4 Systematics tests

4.1 Manipulations of source ellipticities

We performed the following systematics tests:

- The galaxy-cross shear correlation function should be zero, $\gamma_\times(\theta) = 0$. (This has already been investigated in Figure 6).
- Rotate the sources by 45° (i.e., $e_{1,\rm new} = e_{2,\rm old}$ and $e_{2,\rm new} = -e_{1,\rm old}$) and repeat the galaxy-shape cross-correlation function measurement. We should find $\gamma_t(\theta) = 0$.
- Randomize the ellipticities (i.e., randomly shift each pair of values (e_1, e_2) to a different source galaxy). We should find $\gamma_t(\theta) = 0$.
- Replace the lens catalogue by a random catalogue. We should find $\gamma_t(\theta) = 0$.

Figures 15 and 16 show the results of these systematics tests applied to the WiggleZ-RCSLenS and BOSS-RCSLenS cross-correlations and CLONE simulations. The covariance matrices for the measurements are obtained by applying the systematics-test operation to each mock. The χ^2 statistics of the $\gamma_t = 0$ model evaluated using these covariance matrices reveal no evidence for systematic errors.

4.2 Measurement of $\gamma_t(\theta)$ in source redshift slices

We measured $\gamma_t(\theta)$ for WiggleZ and BOSS lenses for sources in photometric redshift bins. We then fit a singular isothermal sphere model $\gamma_t(\theta) = \theta_E/2\theta$, in terms of the Einstein radius

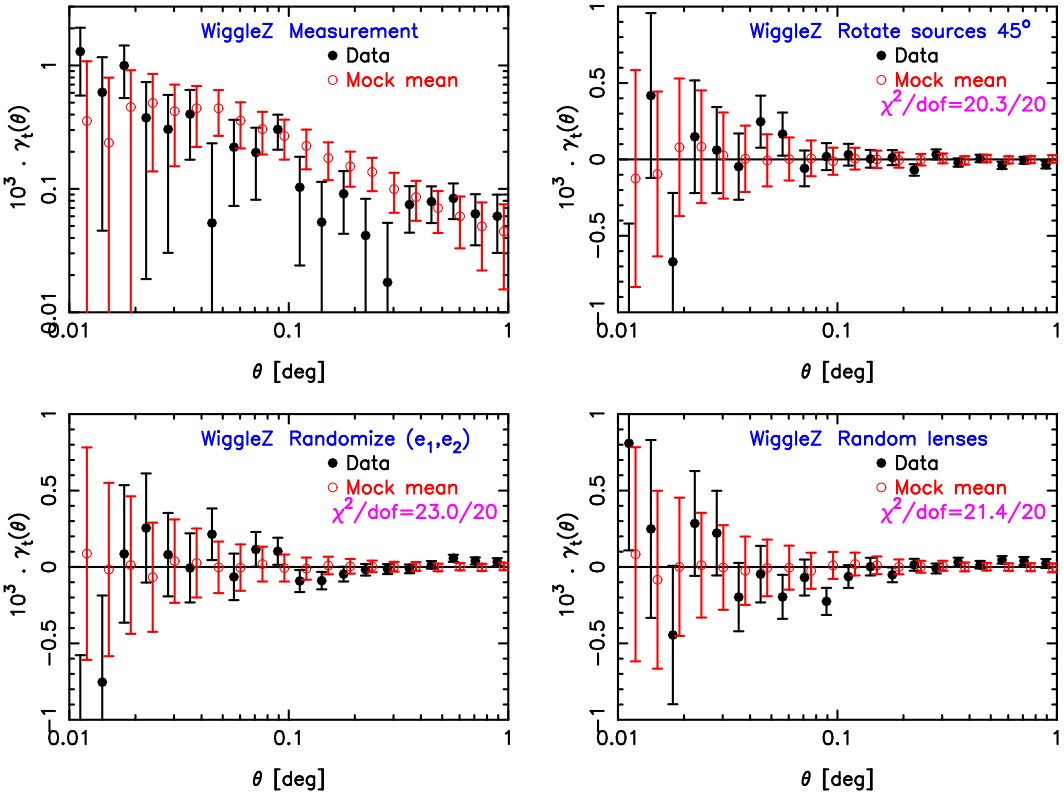

Figure 15: Systematics tests of the $\gamma_t(\theta)$ measurement applied to WiggleZ-RCSLenS cross-correlations. Results are shown for the data and mock mean. χ^2 statistics are quoted for the measurements with respect to a model of zero.

$\theta_E = [4\pi\sigma^2/c^2]\,[(x_s - x_l)/x_s]$, to measurements in the range $0.002 < \theta < 0.2$ deg. Measurements of $\theta_E(z)$ are plotted in Figure 17, along with theoretical predictions for $\sigma = 800$ and 2000 km/s, under the approximation that $z_l = 0.5$. We find that the measurements scale with redshift in the manner predicted by this simple model.

4.3 Measurement of $\gamma_t(\theta)$ with and without cull of pointings with cosmology-independent systematic errors

We repeated the measurements of $\gamma_t(\theta)$ removing RCSLenS pointings flagged as "bad" [$P(U = 0) < 0.05$] by the cosmology-independent systematics analysis. A comparison of the results before and after the cull of pointings is displayed in Figure 18; the results are statistically consistent. *[Note: this needs repeating using the final systematics analysis.]*

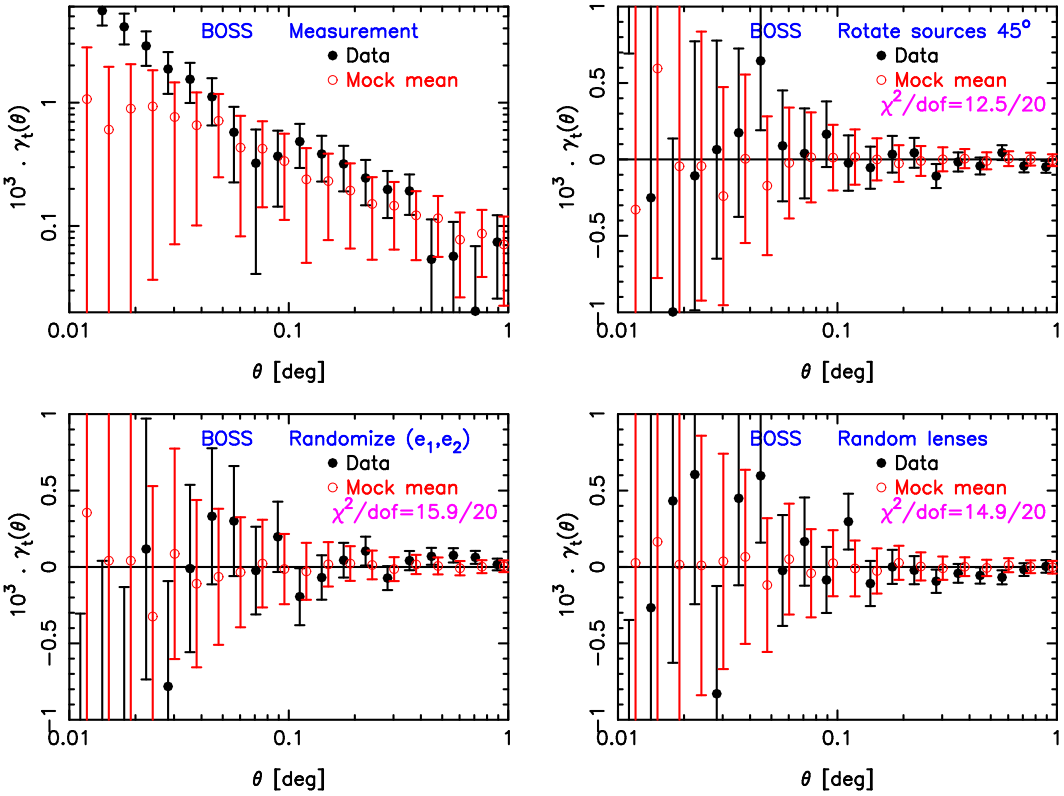

Figure 16: Systematics tests of the $\gamma_t(\theta)$ measurement applied to BOSS-RCSLenS cross-correlations. Results are shown for the data and mock mean. χ^2 statistics are quoted for the measurements with respect to a model of zero.

5 Corrections

5.1 Source-lens association $B(R)$

Owing to photometric redshift errors, some of the sources may be clustered/associated with the lenses. These sources will not be lensed, diluting the cross-correlation signal. The resulting multiplicative bias in the measurement of $\Delta\Sigma(R)$ may be corrected by boosting the signal by

$$B(R) = \frac{\sum_{ls\,\mathrm{pairs}} w_l\, w_s\, w_{ls}}{\sum_{rs\,\mathrm{pairs}} w_r\, w_s\, w_{rs}} \tag{16}$$

where the rs pairs involve random lenses and real sources (with the weights normalized such that $\sum_r w_r = \sum_l w_l$). Figure 19 displays the boost factors $B(R)$ for shapes in the different RCSLenS regions correlated with WiggleZ and BOSS lenses, and the stacked signal optimally combining the regions together. We note that the BOSS lenses have a stronger clustering signal $B(R)$ than the WiggleZ lenses, and that the signal tends to $B(R) = 1$ on large scales.

5.2 Bias due to distribution of lenses with respect to survey boundaries Σ_{rand}

As a systematics test and potential bias correction that should be subtracted from the real measurement if significant, we evaluated the differential projected surface density replacing the data lenses with random lenses, averaging over 10 random catalogues. The result, which we

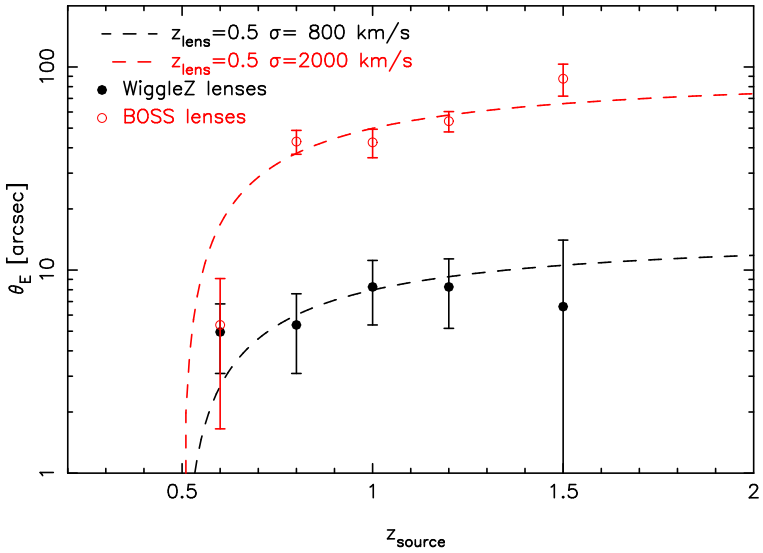

Figure 17: The Einstein radius of WiggleZ and BOSS galaxies as a function of the redshift of the background sources. Theoretical predictions are shown for a singular isothermal sphere model with $\sigma = 800$ and 2000 km/s, making the approximation that $z_l = 0.5$.

denote $\Delta\Sigma_{\rm rand}(R)$, is displayed in Figure 20, which shows shapes in the different RCSLenS regions correlated with WiggleZ and BOSS lenses, and the combined signal. We note that we find no significant non-zero measurement of $\Delta\Sigma_{\rm rand}(R)$, and therefore do not subtract this correction from $\Delta\Sigma(R)$.

5.3 Multiplicative shear bias correction

Bias in the shape measurements is described by a linear combination of a multiplicative error m and an additive error c such that

$$e^{\rm obs} = (1+m)\, e^{\rm true} + c + \text{Noise} \tag{17}$$

The multiplicative correction m has been modelled as a function of source signal-to-noise SN and size in pixels r produced by lensfit:

$$m(SN, r) = \frac{\beta}{\log_{10}(SN)} \exp\left(-r\, SN\, \alpha\right) \tag{18}$$

where $\alpha = 0.0571$ and $\beta = -0.367$. The same correction applies to both e_1 and e_2.

We measure the following correction term for $\gamma_t(\theta)$:

$$1 + K(\theta) = \frac{\sum_{\text{sources}\, i} \sum_{\text{lenses}\, j} w_i^s\, w_j^l\, [1 + m(SN_i, r_i)]\, \Theta(i,j)}{\sum_{\text{sources}\, i} \sum_{\text{lenses}\, j} w_i^s\, w_j^l\, \Theta(i,j)} \tag{19}$$

hence

$$K(\theta) = \frac{\sum_{ls\ \text{pairs}} w_s\, w_l\, m_s}{\sum_{ls\ \text{pairs}} w_s\, w_l} \tag{20}$$

such that the corrected function is given by

$$\gamma_t^{\rm corrected}(\theta) = \frac{\gamma_t^{\rm uncorrected}(\theta)}{1 + K(\theta)} \tag{21}$$

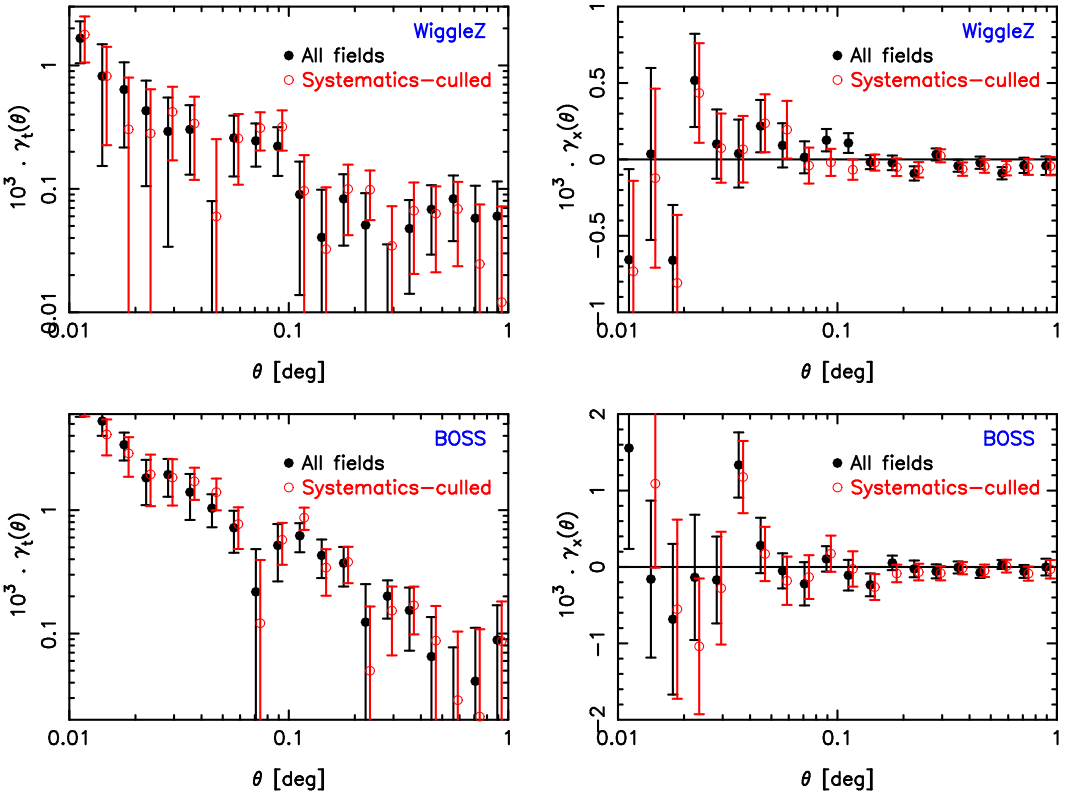

Figure 18: Comparison of measurements of $\gamma_t(\theta)$ and $\gamma_\times(\theta)$ including and excluding fields flagged with systematics.

The analogous formula for the correction to be applied to $\Delta\Sigma(R)$ is

$$1 + K(R) = \frac{\sum_{ls\,\mathrm{pairs}} w_l\, w_s\, w_{ls}\, [1 + m_s]\, K_{ls}}{\sum_{ls\,\mathrm{pairs}} w_l\, w_s\, w_{ls}\, K_{ls}} \tag{22}$$

where $K_{ls} \propto \Sigma_c(z_s, z_l)$ is defined above, hence

$$K(R) = \frac{\sum_{ls\,\mathrm{pairs}} w_l\, w_s\, K_{ls}^{-1}\, m_s}{\sum_{ls\,\mathrm{pairs}} w_l\, w_s\, K_{ls}^{-1}} \tag{23}$$

such that the corrected function is given by

$$\Delta\Sigma^{\mathrm{corrected}}(R) = \frac{\Delta\Sigma^{\mathrm{uncorrected}}(R)}{1 + K(R)} \tag{24}$$

Figure 21 displays the corrections measured for the different WiggleZ and BOSS regions; we find that $K \approx -0.04$.

5.4 Additive shear bias correction

The measurement of e_2 contains a bias c_2. Figure 22 shows measurements of $\gamma_t(\theta)$ for WiggleZ and BOSS fields excluding and including the c_2 correction; the difference between the results is negligible.

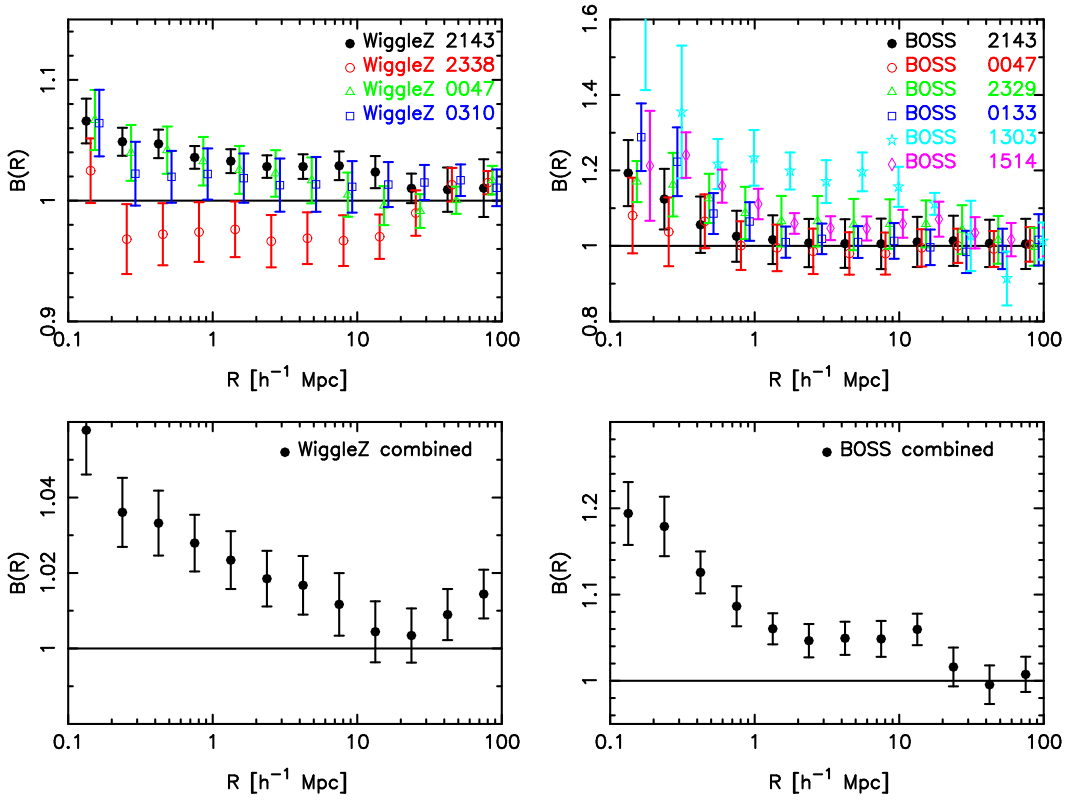

Figure 19: Boost factor $B(R)$ from source-lens clustering for WiggleZ regions (top left), BOSS regions (top right), WiggleZ data combined (bottom left), BOSS data combined (bottom right).

5.5 Photometric-redshift dilution

Photometric redshift errors cause a dilution in the measurements of $\Delta\Sigma(R)$; for example, a source galaxy which is in reality in front of a lens can be scattered to lie behind it, and be included in the measurement when in reality it is adding no signal. We used the CLONE mock catalogues to model three types of source photo-z error:

- A Gaussian photo-z error with standard deviation $\sigma_z = 0.2(1+z)$.
- An internal scrambling of the array of source redshifts, such that each photo-z is randomly replaced with another drawn from the overall distribution.
- The full photo-z error distribution $P(z_p|z_s)$, determined above, is applied to each mock.

The mock mean of $\Delta\Sigma(R)$ measurements, corresponding to each of these photo-z error models, is displayed in Figure 23, comparing the WiggleZ and BOSS lens redshift distributions. *[Note: I have not yet decided whether to apply these effects as a correction to the data or model.]*

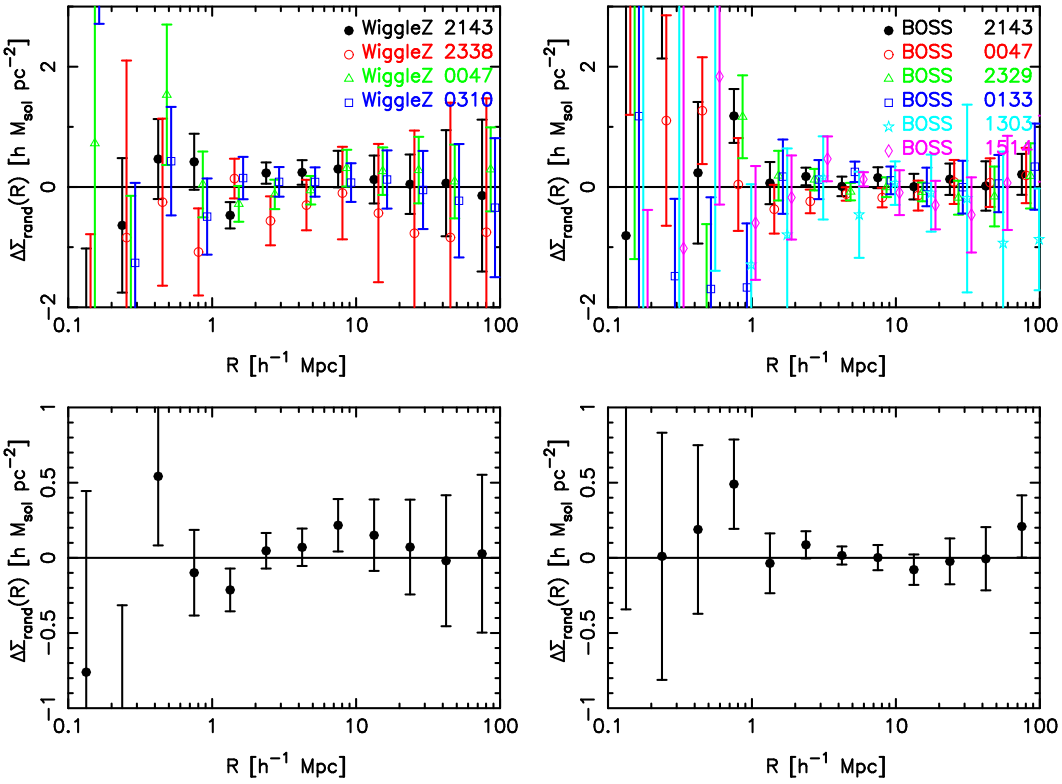

Figure 20: Cross-correlation between shapes and random lenses, $\Delta\Sigma_{\rm rand}(R)$, for WiggleZ regions (top left), BOSS regions (top right), WiggleZ data combined (bottom left), BOSS data combined (bottom right).

6 Cosmology fits

6.1 Models

The following equations indicate how to model the tangential shear signal $\gamma_t(\theta)$ for a given cosmological model and redshift distributions of sources and lenses. Notation: $x(z)$ is the co-moving radial co-ordinate at redshift z, $P(k,z)$ is the non-linear matter power spectrum obtained using CAMB+halofit, $a(z) = 1/(1+z)$ is the cosmic scale factor, $[p_{\rm shape}(z), p_{\rm density}(z)]$ are the redshift probability distributions of the shape and density samples normalized such that $\int_0^\infty p(z)\,dz = 1$, b is the bias factor of the density sample. Approximations: Limber equation, neglect cosmic magnification and intrinsic alignments, flat Universe.

$$\gamma_t(\theta) = \frac{1}{2\pi}\int_0^\infty d\ell\,\ell\,P_{g\kappa}(\ell)\,J_2(\ell\theta) \tag{25}$$

$$P_{g\kappa}(\ell) = b\left(\frac{3\,\Omega_{\rm m}\,H_0^2}{2\,c^2}\right)\int_0^\infty dz\,\frac{dx}{dz}\,\frac{1}{a(z)}\,P\left(\frac{\ell}{x(z)}, z\right)\,W_{\rm shape}(z)\,W_{\rm density}(z) \tag{26}$$

$$W_{\rm shape}(z) = \int_z^\infty dz'\,p_{\rm shape}(z')\left(\frac{x(z')-x(z)}{x(z')}\right) \tag{27}$$

$$W_{\rm density}(z) = \frac{p_{\rm density}(z)}{x(z)\frac{dx}{dz}} \tag{28}$$

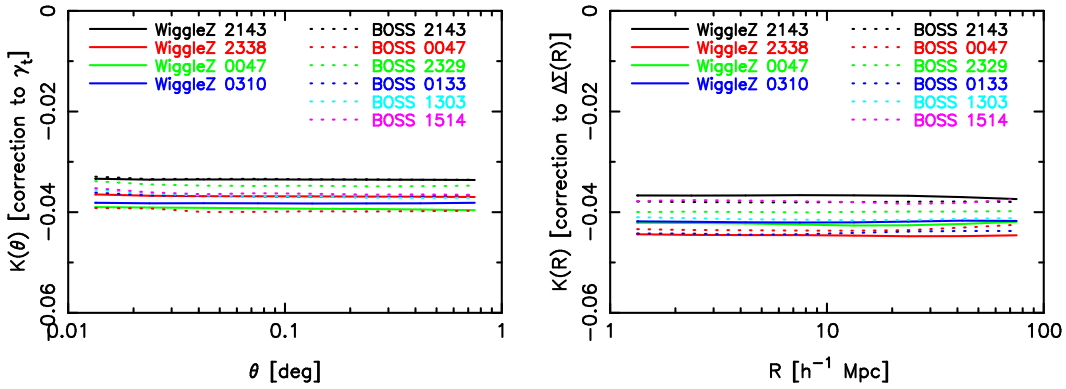

Figure 21: Multiplicative shear bias corrections to be applied to $\gamma_t(\theta)$ (left-hand panel) and $\Delta\Sigma(R)$ (right-hand panel), determined for the different survey regions.

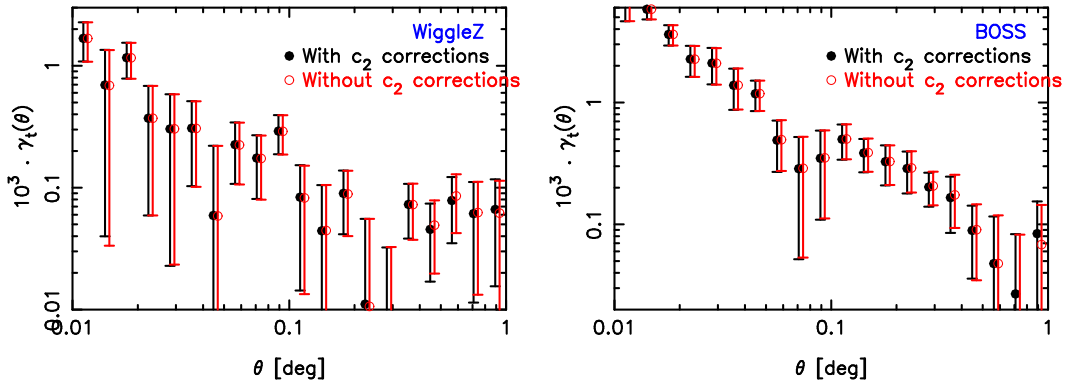

Figure 22: Measurements of $\gamma_t(\theta)$ for WiggleZ and BOSS fields excluding and including the c_2 correction.

The following equations indicate how to model the differential projected surface density $\Delta\Sigma(R)$ for a given model galaxy-mass correlation function $\xi(r)$. We note that

$$\Sigma(R) = \int \xi(\sqrt{R^2+\pi^2})\, d\pi = \int_R^\infty \frac{x\,\xi(x)\,dx}{\sqrt{x^2-R^2}} \tag{29}$$

and

$$\int_0^R R'\,\Sigma(R')\,dR' = \int_0^R R'\,dR' \int_{R'}^\infty \frac{x\,\xi(x)\,dx}{\sqrt{x^2-R'^2}} \tag{30}$$

$$= \int_R^\infty dx\,x\,\xi(x) \int_0^R \frac{dR'\,R'}{\sqrt{x^2-R'^2}} + \int_0^R dx\,x\,\xi(x) \int_0^x \frac{dR'\,R'}{\sqrt{x^2-R'^2}} \tag{31}$$

$$= \int_0^\infty x^2\,\xi(x)\,dx - \int_R^\infty x\sqrt{x^2-R^2}\,\xi(x)\,dx \tag{32}$$

and hence

$$\Delta\Sigma(R) = \frac{2}{R^2}\int_0^\infty x^2\,\xi(x)\,dx - \frac{2}{R^2}\int_R^\infty x\sqrt{x^2-R^2}\,\xi(x)\,dx - \int_R^\infty \frac{x\,\xi(x)\,dx}{\sqrt{x^2-R^2}} \tag{33}$$

6.2 Validation of the methodology using the CLONE simulations

Models of $\gamma_t(\theta)$ and $\Delta\Sigma(R)$ were computed for the CLONE mock catalogues, incorporating the finite-box size corrections mentioned above. The models were then fitted to each of the 20

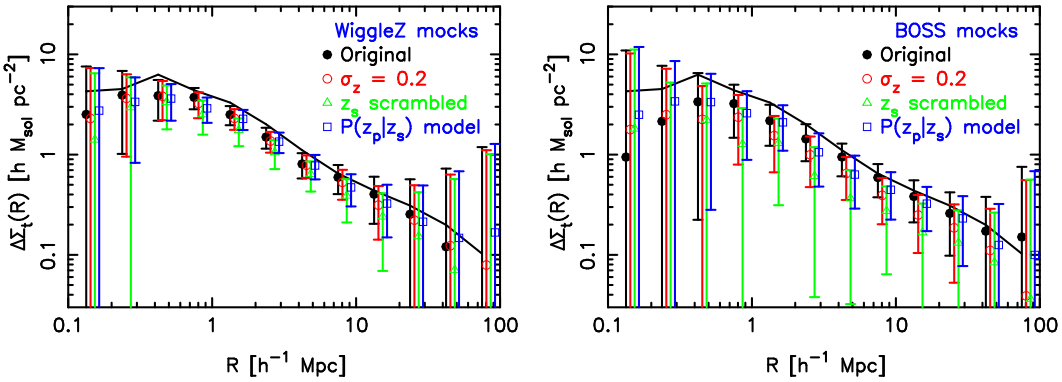

Figure 23: Measurements of $\Delta\Sigma(R)$ for WiggleZ and BOSS CLONE mocks, applying various forms of photo-z error distribution to the source catalogues.

CLONE realizations incorporating the survey selection functions, using the area-scaled covariance matrices determined from the 184 lines-of-sight, varying a single bias factor. Fits were performed for WiggleZ lenses in redshift slices ($0.2 < z < 0.6, 0.4 < z < 0.8, 0.6 < z < 0.9$) and BOSS lenses ($0.43 < z < 0.7$). Figure 24 shows, for each of these samples, the combined probability distributions of the fitted bias factors across the 20 realizations (solid black line) and the distribution of the 20 best-fitting values (red histogram) compared to the input bias factors of the mocks (vertical dotted lines). The pipeline successfully recovers the input bias factors.

Figure 25 displays a similar set of tests applied to the measurements of the projected cross-correlation functions $\Delta\Sigma(R)$; the input bias factors are again successfully recovered. In Figure 26 we introduce the photo-z error models defined above, illustrating the resulting dilution of clustering that causes a downward bias in the fitted amplitudes.

6.3 E_G parameter

[Note: This work is on hold awaiting the data and mocks to be finalized].

We can determine

$$E_G(R) = \frac{1}{\beta}\frac{\Upsilon_{gm}(R, R_0)}{\Upsilon_{gg}(R, R_0)} \tag{34}$$

for the WiggleZ and BOSS samples, using the values of β quoted in their respective redshift-space distortion analyses.

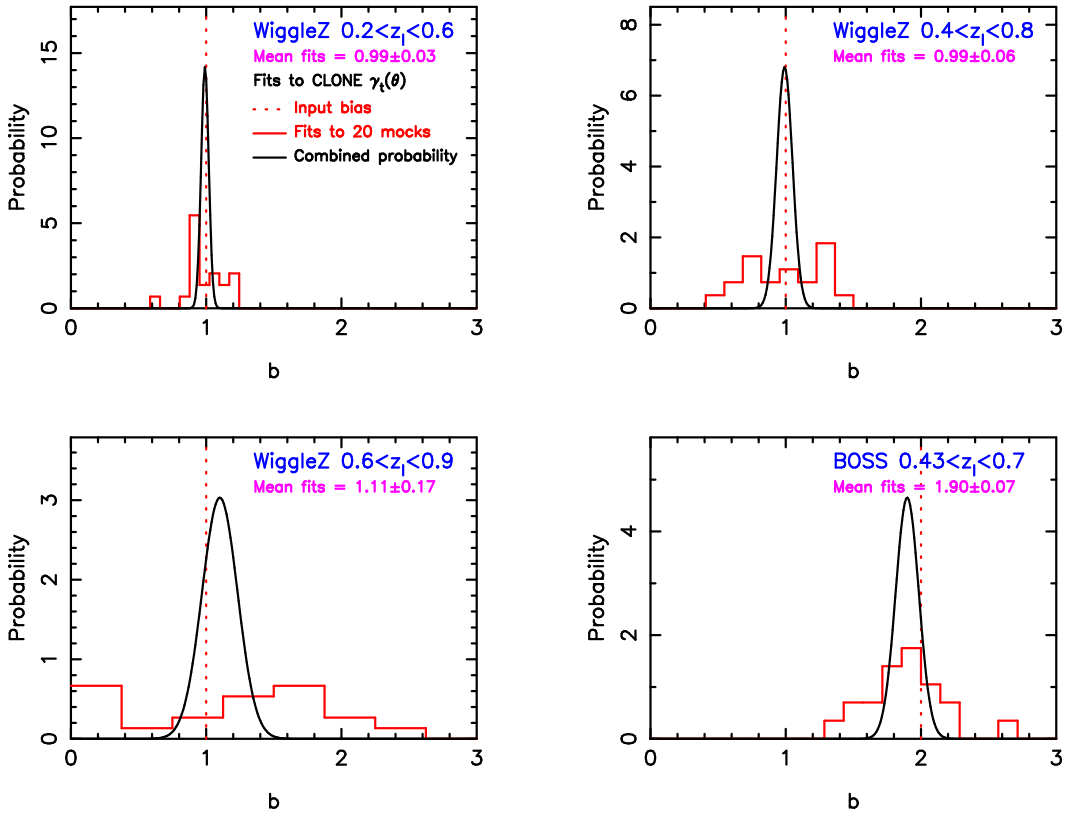

Figure 24: Bias fits to the $\gamma_t(\theta)$ measurements of 20 full-survey realizations of CLONE mocks for WiggleZ lenses in redshift slices ($0.2 < z < 0.6, 0.4 < z < 0.8, 0.6 < z < 0.9$) and BOSS lenses ($0.43 < z < 0.7$). The solid black line is the combined posterior probability distributions of the bias factors for the 20 realizations, the red histogram is the distribution of the 20 best-fitting values, and the vertical dotted line is the input bias factor of the mocks.

7 Task list

- Update analysis to BOSS DR10 sample when publicly available.
- Finalize cosmology-independent systematics tests for RCSLenS sample.
- Finalize source redshift distributions to be used for the whole sample and photo-z sample. Re-generate the mock catalogues using these new distributions.
- Change approach for measuring $\Delta\Sigma(R)$ such that it does not assume a bias and growth model.
- Finalize photo-z correction to $\Delta\Sigma(R)$ and complete measurement of E_G.
- When satisfied with tests using the mock catalogues, run the σ_8 and bias fits on the data samples.

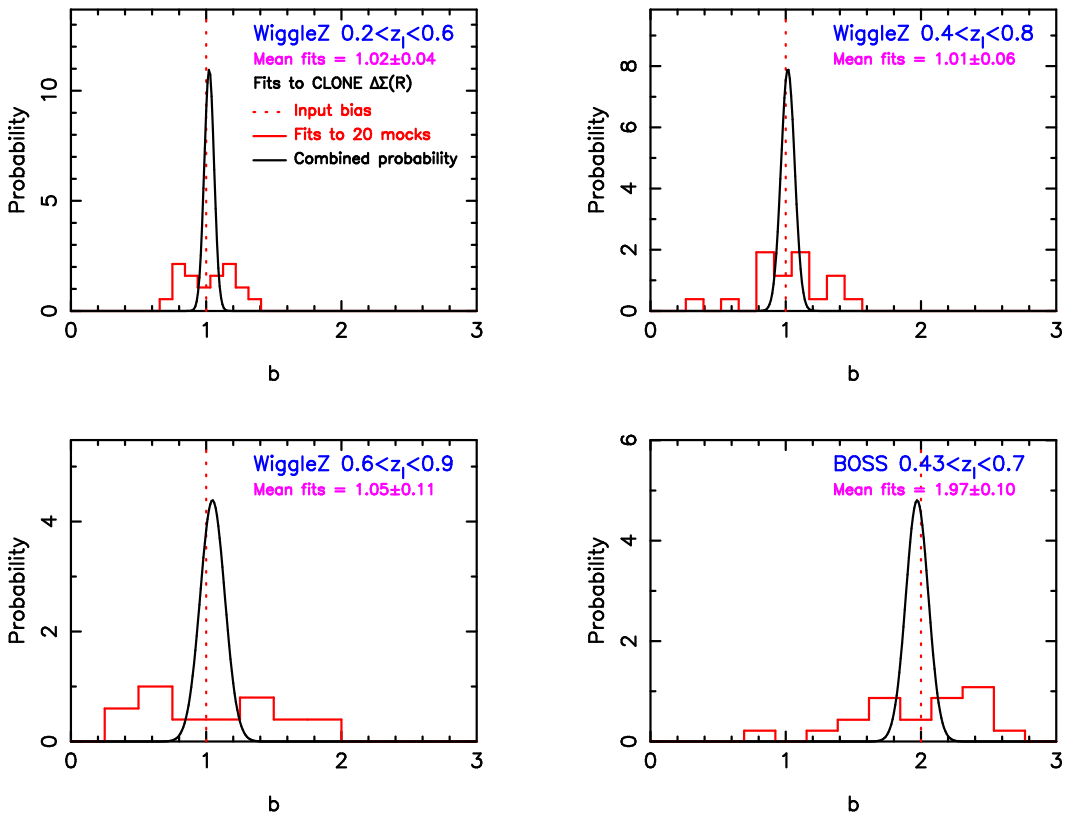

Figure 25: Similar tests to Figure 24, fitting to the projected cross-correlations $\Delta\Sigma(R)$ of each mock catalogue.

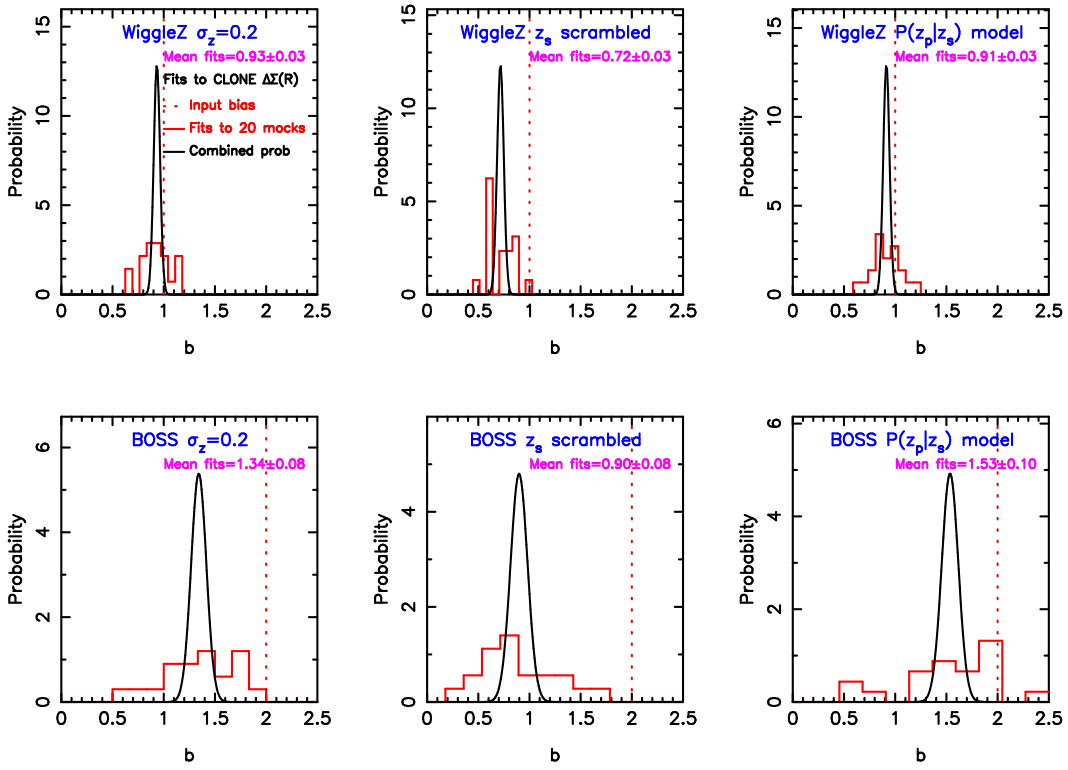

Figure 26: Similar tests to Figure 24, fitting to the projected cross-correlations $\Delta\Sigma(R)$ of each mock catalogue including various photo-z error models. In these cases the best-fitting amplitudes lie below the input bias factor of the mock.